Large-eddy simulation analysis of knock in a direct injection spark ignition engine

Anthony Robert, Karine Truffin, Nicolas Iafrate, Stéphane Jay, Olivier Colin, Christian Angelberger

Journal Title
XX(X):1–11

DOI: 10.1177/ToBeAssigned
www.sagepub.com/
SAGE

Large-eddy simulation analysis of knock in a direct injection spark ignition engine

A. Robert[1], K. Truffin[1], N. Iafrate[1], S. Jay[1], O. Colin[1] and C. Angelberger [1]

Abstract

Downsized spark ignition (SI) engines running under high loads have become more and more attractive for car manufacturers because of their increased thermal efficiency and lower CO2 emissions. However, the occurrence of abnormal combustions promoted by the thermodynamic conditions encountered in such engines limits their practical operating range, especially in high efficiency and low fuel consumption regions. One of the main abnormal combustion is knock, which corresponds to an autoignition of end gases during the flame propagation initiated by the spark plug. Knock generates pressure waves which can have long term damages on the engine, that is why the aim for car manufacturers is to better understand and predict knock appearance. However an experimental study of such recurrent but non-cyclic phenomena is very complex, and these difficulties motivate the use of CFD for better understanding them.

In the present paper, Large-Eddy Simulation (LES) is used as it is able to represent the instantaneous engine behavior and thus to quantitatively capture cyclic variability and knock. The proposed study focuses on the LES analysis of knock for a direct injection SI engine. A spark timing sweep available in the experimental database is simulated, and 15 LES cycles were performed for each spark timing. Wall temperatures, which are a first order parameter for knock prediction, are obtained using a conjugate heat transfer study. Present work points out that LES is able to describe the in-cylinder pressure envelope whatever the spark timing, even if the sample of LES cycles is limited compared to the 500 cycles recorded in the engine test bench. The influence of direct injection and equivalence ratio stratifications on combustion is also analyzed. Finally, focusing on knock, a MAPO (Maximum Amplitude Pressure Oscillation) analysis is conducted for both experimental and numerical pressure traces pointing out that LES well reproduces experimental knock tendencies.

Keywords

Knock, LES, Direct injection, Downsized engine, MAPO

Introduction

In the last decade, downsized spark ignition (SI) engines running under high loads behave attracted increasing interest thanks to their increased thermal efficiency and low CO2 emissions. However, the related high engine loads induce severe thermodynamic conditions in the combustion chamber, promoting the occurrence of abnormal combustions like knock. This phenomenon is related to an uncontrolled auto-ignition (AI) of the fresh gases before their consumption by the premixed flame initiated by the spark ignition device. It highly depends on the current combustion velocity as well as species composition and temperature fluctuations in the cylinder, making knock a recurrent but non-cyclic phenomenon.

The detailed study of knock is experimentally complex because of the confined geometry and their possible destructive characteristics. Such limitations motivate the use of CFD for better understanding these specific combustions. Notably, RANS simulations were used to predict and understand the occurrence of knock (1; 2). However, the RANS approach is limited to the description of the mean cycle, which is not always affected by knock because of its sporadic nature. Large-Eddy Simulation (LES) appears as an attractive alternative because it allows the simulation of individual cycles, thus reproducing the link between knock and cyclic variability. In the last few years, first attempts were made to model these phenomena (3; 4; 5), demonstrating the potential of LES to address this topic. More recent work addressed first quantitative comparisons of LES results with experimental data (6), pointing out that LES is able to predict knock tendencies. LES also allows analyzing in detail the occurrence of knocking events. Low knock intensity is linked to one or several local auto-ignition spots which consume only the surrounding fresh gases, whereas the occurrence of a transition from deflagration to detonation is responsible for the highest knock intensities observed in SI engines (7). The present paper addresses for the first time a quantitative LES study of knocking combustion in a SI engine, accounting for the direct injection and accurate wall temperature boundary conditions.

[1]IFP Energies nouvelles, 1 et 4 avenue de Bois-Préau 92852 Rueil Malmaison, France ; Institut Carnot IFPEN Transports Energie

Corresponding author:
Anthony Robert, IFP Energies nouvelles, 1 et 4 avenue de Bois-Préau 92852 Rueil Malmaison, France ; Institut Carnot IFPEN Transports Energie
Email: anthony.robert@ifpen.fr

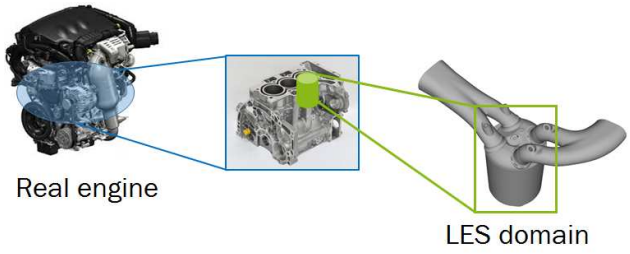

Figure 1. Presentation of the real engine configuration and the LES computation domain.

A spark timing variation available in the experimental database is simulated in LES. The effect of injection on the mixture formation and in particular on equivalence ratio heterogeneity at spark timing is studied. The flow around the spark plug is then analyzed and observations are linked to the combustion behavior. Finally, the knock tendency as a function of the spark timing predicted by LES is compared with experimental trends.

EXPERIMENTAL SET-UP

The original engine configuration is a three cylinder four-valve engine from groupe PSA, and the computational domain corresponds to one single cylinder chosen amongst them, as shown in Fig. 1.

The configuration is a direct injection spark ignition engine, whose features are summarized in Tab. 1. The operating point is at 5500 rpm with an IMEP of 19 bars. The fuel is a commercial European gasoline (SP95-E10) with 10% of volume fraction of ethanol. This fuel is injected thanks to an asymmetric five holes injector using a single injection occurring early during the intake phase in order to obtain a mixture as premixed as possible at top dead center (TDC). A spark timing (ST) sweep is available in the experimental database, and for confidentiality issues, spark timing values are given in this article relative to the latest spark timing called “reference spark timing”.

Table 1. Engine characteristics and simulated operating point.

Engine capacity	400cc
Compression ratio	10.3
Rotational speed	5500 RPM
IMEP	19 bar
Fuel	SP95-E10
Injection timing	Early during the cycle
Spark timing sweep	From -7,5 CAD before the reference spark timing to the reference ST

MESHES AND BOUNDARY CONDITIONS FOR LES

Seventy tetrahedral meshes are needed to simulate a full cycle, owning between 1.7 and 9.2 Million cells. The LES methodology used for the moving mesh is described in (8). The mean cell size is approximately 0.05mm at the residual lift for intake and exhaust valves. Cell size in the chamber is around 0.7mm during the main part of the cycle and 0.5mm during combustion phases. Finally, the mesh size is refined down to 0.2mm in the vicinity of the spark plug during ignition. Several meshes are presented in Fig. 2.

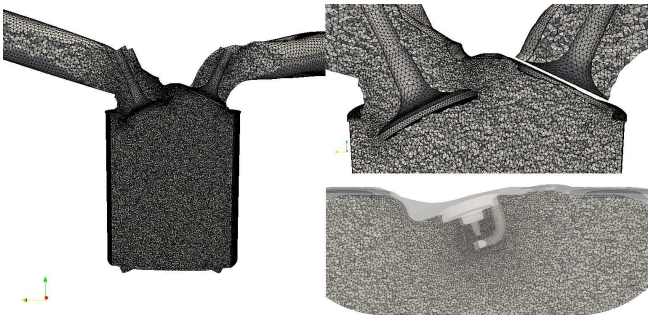

Figure 2. Presentation of meshes used during intake valve opening (left and top right) and at the spark plug during ignition (bottom right).

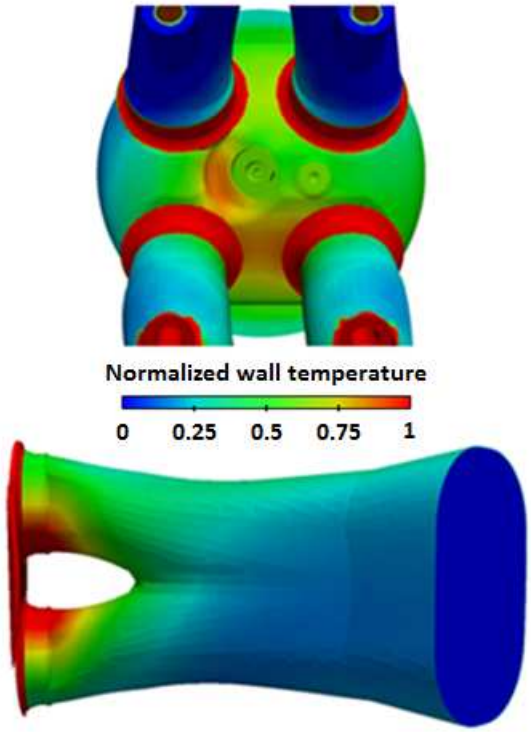

Figure 3. Normalized wall temperatures imposed as LES boundary conditions for cylinder head and intake pipe.

At the inlet and outlet of the LES domain, boundary conditions are handled using the NSCBC approach (9; 10). The same temporal signals resulting from a GT-power calculation are imposed as boundary conditions for each LES cycle.

Wall temperatures, which are a first order parameter to study knock, are estimated using a conjugate heat transfer (CHT) based on RANS calculations. Computed temperature fields are imposed as wall boundary conditions in LES. Fig. 3 presents the resulting normalized wall temperature distribution for the cylinder head and the intake pipe. The hot region visible on the cylinder head is thus taken into account. Owing to the strong thermal inertia, these wall temperatures were kept constant for all simulated LES cycles. The valves were not included in CHT study, and their temperatures are

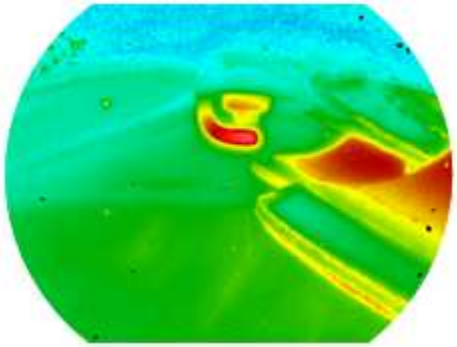

Figure 4. Thermal image of the exhaust valves.

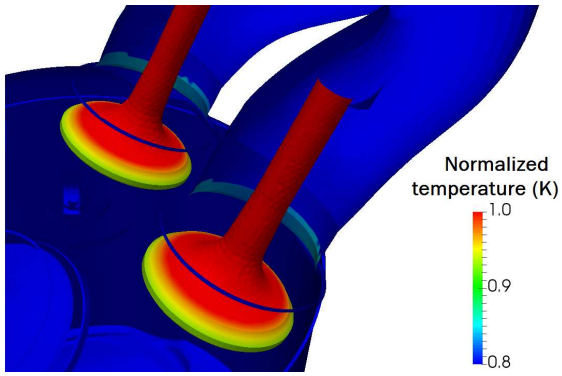

Figure 5. LES wall temperatures of exhaust valves.

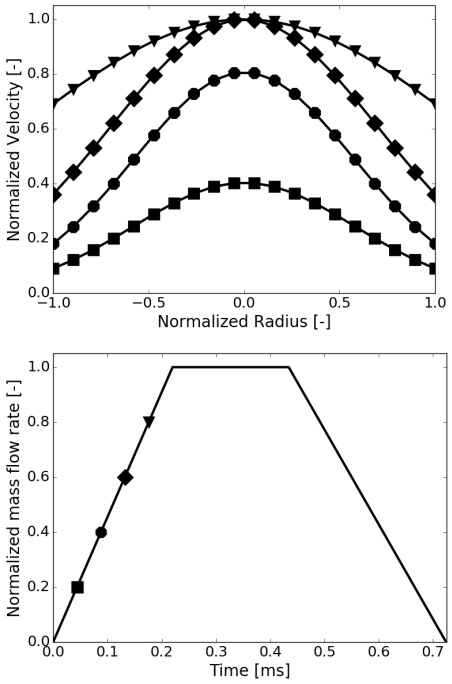

Figure 6. Example of adapted normalized velocity profiles (top) depending on the instantaneous injected mass flow rate (bottom)

estimated using thermal images of the real engine test bench (Fig. 4). They are then imposed in the LES calculations with a temperature gradient on the edges of the valves (Fig. 5) to approximate the heat exchange at the valve seats during valves closure.

NUMERICAL SET-UP

Large-Eddy Simulations are performed using the AVBP code (8; 11), co-developed and co-owned by CERFACS and IFPEN. AVBP solves the multi-species, compressible, reactive Navier-Stokes equations on unstructured and moving meshes (10). Time advancement is explicit and convection is discretized in the present simulations using a second-order (in space and time) centered finite volume Lax-Wendroff scheme (12). The subgrid scale turbulence is modeled by a Smagorinsky model (13) with a constant set to Cs=0.18. Finally, the wall shear stress and heat flux are imposed using a RANS modeling based on a logarithmic law-of-the-wall (14).

The Lagrangian formalism (15) is used to represent the liquid phase. Due to the diluted liquid phase assumption, droplets injected are smaller than flow characteristics scales and the point source approximation is employed. To initiate the spray physics at the nozzle exit, a simple disk model is used (16). This model assumes that injected liquid can be described with a discrete approach omitting the dense region of the spray. A full disk surface is defined at the nozzle exit, on which a random deposit of particle is made. The main idea is to define a Gaussian velocity profile in order to conserve momentum. The following equation is verified:

$$\iint_{S_{inj}} \rho_p.m_l.r.V_{mean}.dr.d\theta = \iint_{S_{inj}} \rho_p.m_l.r.V(r).dr.d\theta \quad (1)$$

Where m_l, S_{inj}, V_{mean} and r represent respectively the liquid mass, injection disk surface, mean velocity and position on the disk. Assuming a constant liquid density and an independence between the liquid mass and the injection area, it can be rewritten as follow:

$$\iint_{S_{inj}} r.V_{mean}.dr.d\theta = \iint_{S_{inj}} r.V(r).dr.d\theta \quad (2)$$

V_{mean} is computed from the instantaneous injection rate Q_{inj}:

$$V_{mean}(t) = \frac{Q_{inj}}{S_{inj}\alpha_l\rho_p} \quad (3)$$

Where α_l is the cavitation coefficient.
The Gaussian velocity profile $V(r)$ is defined by:

$$V(r) = V_{max}\exp(-\sigma r^2) \quad (4)$$

The maximal velocity is located at the center of the disk, and is:

$$V_{max} = \frac{\sigma V_{mean}}{1-\exp(-\sigma)} \quad (5)$$

To respect physical properties, the maximum velocity is limited by the Bernoulli velocity. As a consequence, the Gaussian parameter σ is adjusted to conserve momentum (Fig. 6).

Finally a turbulent fluctuation at the nozzle exit is introduced by adding a random velocity contribution to the normal and radial liquid velocity, as:

$$V(r,\theta) = V(r)(1 + 2V_{rms} * RN) \quad (6)$$

Where θ is the angular position on the injection disk surface, V_{rms} a given dimensionless velocity fluctuation and RN a random number between 0 and 1 different for each position (r,θ).

The flame front propagation is described using the ECFM-LES premixed combustion model (8; 17; 18). The local mean laminar flame speed is obtained from the correlation of Yahyaoui et al. (19) that was developed for various mixtures of gasoline/ethanol. The spark ignition is modeled using the ISSIM-LES model (20) which includes the description of the electrical circuit and 3D modeling of the flame kernel growth during ignition. The tabulated auto-ignition model (TKI-LES) (6; 21) is used to model the reaction rate linked to the occurrence of auto-ignition in the fresh gases. This model is based on a progress variable that is independent of the premixed flame one. Both phenomena are therefore fully decoupled so that an auto-ignition spot does not create artificially a propagating flame. The TKI model uses a look-up table built from complex chemistry simulations using a TRF surrogate with 42.8% isooctane, 13.7% n-heptane, 43.5% toluene and the LLNL kinetic mechanism considering 1388 species and 5935 reactions (22). Based on local conditions, an auto-ignition reaction rate is extracted from the TKI table for each node of the mesh, and used in the species transport equations.

The post-flame kinetics is taken into account to correct the burned gases state and temperature. First the remaining fuel that has not been consumed by the propagating flame can be post-oxidized using the following consumption rate model:

$$\widetilde{\omega}_{F^b} = \overline{\rho} W_F A' \exp\left(-\frac{E_a'}{RT_b}\right)\left(\frac{\overline{\rho}\widetilde{Y}_F^b}{W_F}\right)^{0.55}\left(\frac{\overline{\rho}\widetilde{Y}_{O_2}^b}{W_{O_2}}\right)^{0.9} \quad (7)$$

with $A' = 6.10^{11}$ cm^3.mol^{-1}.s^{-1} and $E_a' = 41500$ cal.mol^{-1}. The b exponent stands for the burnt gas state.

Second the kinetic oxidation of CO is also introduced:

$$CO + \tfrac{1}{2}O_2 \leftrightarrow CO_2 \quad (8)$$

The rate of reaction of Eq. 8 is given by:

$$Q = k_f\left(\frac{\overline{\rho}\widetilde{Y}_{CO}^b}{W_{CO}}\right)\left(\frac{\overline{\rho}\widetilde{Y}_{O_2}^b}{W_{O_2}}\right)^{1/2} - k_r\left(\frac{\overline{\rho}\widetilde{Y}_{CO_2}^b}{W_{CO_2}}\right) \quad (9)$$

with W_{CO}, W_{CO_2} and W_{O_2} the molar mass of CO, CO2 and O2 respectively, and $\widetilde{Y}_{CO}^b$, $\widetilde{Y}_{CO_2}^b$, $\widetilde{Y}_{O_2}^b$ their mass fractions in the burnt gases. k_f and k_r are the forward and reverse reaction rates:

$$k_f = A\exp\left(-\frac{E_a}{RT_b}\right) \text{ and } k_r = \frac{k_f}{K_{eq}} \quad (10)$$

where the pre-exponential constant A is fixed to 9.10^8 cm^3.mol^{-1}.s^{-1} , the activation energy is 40000 cal.mol^{-1} and K_{eq} is the equilibrium constant defined by (23). The rate constants of this reduced two-step mechanism were adjusted to recover the correct heat release rate and burned gases temperature on homogeneous auto-ignition reactor calculations at various fuel/air ratios and pressures. For this purpose the same LLNL mechanism used to generate the TKI table was used as a reference solution.

Figure 7. Image of injected droplets in the cylinder during intake valve opening for one LES cycle. Droplets are colored by their temperature.

RESULTS AND DISCUSSIONS

Fifteen consecutive cycles for the reference spark timing (the latest one of the ST sweep) were first simulated with LES.

Reference spark timing analysis

The simulated operating point owns an early injection illustrated on Fig. 7. Fuel is injected during intake valve opening, droplets are driven into the tumble motion and this type of injection should lead to a premixed mixture at TDC. To analyze injection in more details, Fig. 8 shows the temporal evolution of the liquid mass in the combustion chamber, which increases during injection before reaching a maximum value around -200 CAD before TDC. Liquid masse then decreases due to the evaporation of droplets which are fully evaporated around 60 CAD bTDC.

Fig. 9 shows the distribution of local fuel/air equivalence ratio in the chamber at three different instants for the simulated cycles. The mixing resulting from the compression of the tumbling intake flow, reduces the spatial variations as one comes close to TDC, where it centers around the targeted mean equivalence ratio of 1.2.

However, the mixture is not fully homogeneous at TDC, exhibiting a non-negligible instantaneous stratification, and shows important cycle-to-cycle variability. Fig. 10 shows the spatial distributions for cycles 2 and 10 at TDC, which are two extreme ones in terms of mixture heterogeneity in the LES cycles. The spatial variance of equivalence ratio for cycle 10 is higher than for cycle 2, with equivalence ratio extrema going from 0.9 to 1.6, which is much more heterogeneous than cycle 2. It is important to notice that cycle 2 is one of the most homogeneous LES cycles.

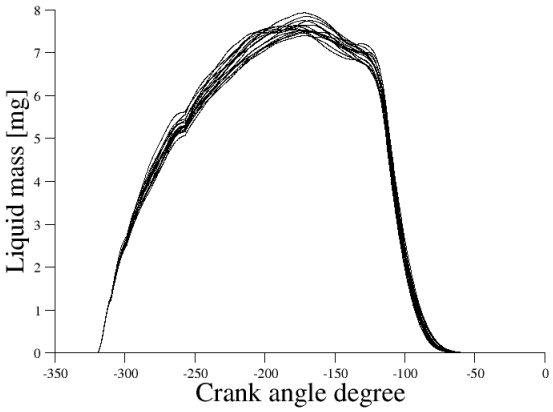

Figure 8. Temporal evolution of liquid mass for the fifteen LES cycles at the reference ST.

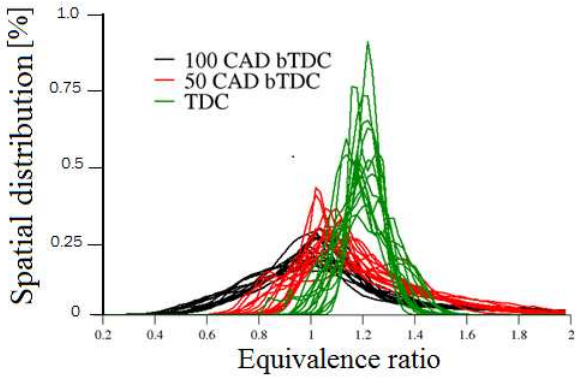

Figure 9. Spatial distribution of equivalence ratio for fifteen LES cycles at three instants during compression.

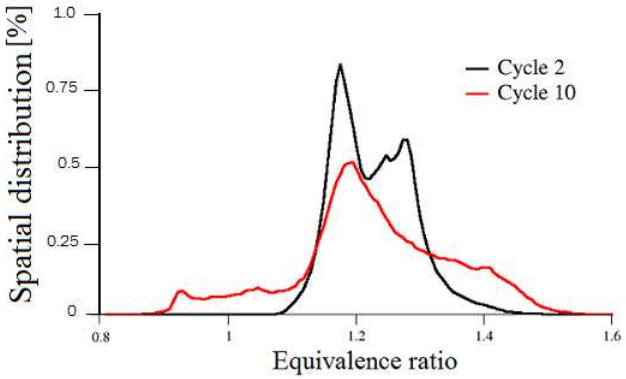

Figure 10. Spatial distribution at TDC for two individual cycles at the reference ST.

These observations are confirmed on Fig. 11 where equivalence ratio on a horizontal cut plane at TDC is presented for the same LES cycles. The spatial distribution of equivalence ratio is much smaller for cycle 2 than for cycle 10. Overall, the LES predictions indicate that a perfectly premixed fuel/air mixture is not obtained at TDC.

Despite the found strong differences in mixture homogeneity between cycles 2 and 10, this is not sufficient

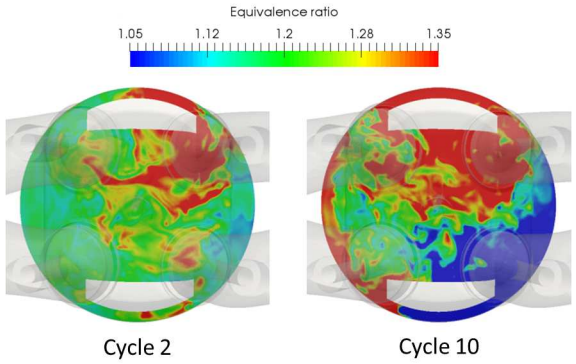

Figure 11. Comparison of equivalence ratio fields on a horizontal cut plane at TDC for two LES cycles.

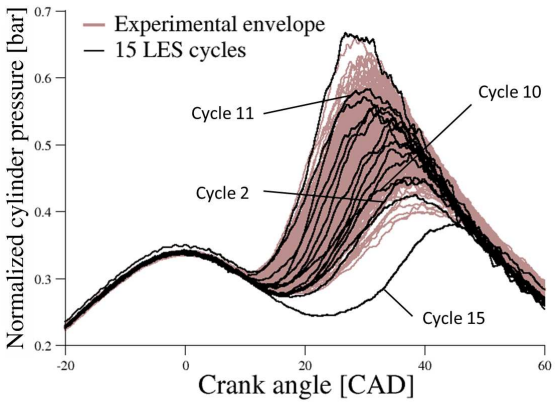

Figure 12. Normalized in-cylinder pressure comparison between LES (black) and experiment (brown) at the reference spark timing.

to explain the predicted cyclic combustion variability. As shown in Fig. 12, these two extreme cycles in terms of heterogeneity are indeed not extreme in terms of combustion speed, as both are located in the bottom part of the cylinder pressure envelope. Overall the cyclic combustion variability predicted by the 15 LES cycles reproduces quite well the one observed experimentally based on 500 cycles. Note that the reported pressure was recorded at the same position in experiments and LES.

However, it may be noticed that LES cycle number 15 lies below the statistically probable envelope of the experiments, right after the spark ignition timing. To understand what happens in more details, Fig. 13 and Fig. 14 show the mean equivalence ratio and flow velocity magnitude in a sphere of 5 mm around the spark plug at the instant of spark ignition. Values are plotted over the cycle identification number, and we can first notice that cycle 1 is not taken into account as results depend too much on the initial condition.

The mean equivalence ratio is fluctuating around the mean value of 1.2, with limited cycle-to-cycle variability. In particular the mean equivalence ratio at the spark of cycle 15 is very close to the one for cycle 11 which is the second fastest cycle predicted in LES (see Fig. 12). On the other hand, cycle 2 and 10 have different mean equivalence ratios at the spark plug but exhibit very similar combustion speeds. It appears that despite the fact that equivalence ratio at the

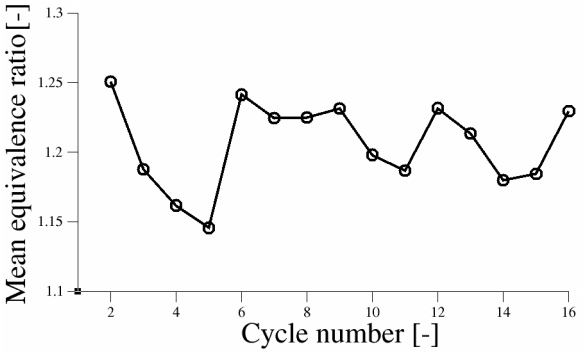

Figure 13. Mean equivalence ratio at the spark plug for the fifteen LES cycles at the reference spark timing.

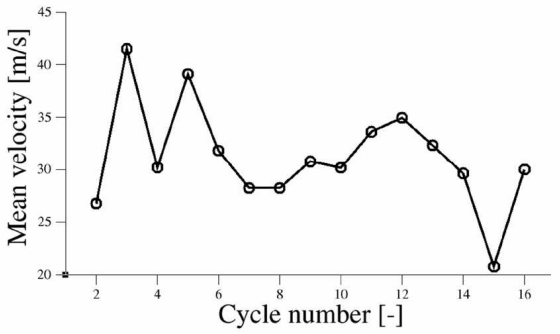

Figure 14. Mean velocity magnitude at the spark plug for the fifteen LES cycles at the reference spark timing.

spark plug is one of the parameters influencing the ignition phase and combustion development, its cyclic variability does not appear to be sufficient to explain the combustion variability. Fig. 14 shows that the cycle-to-cycle variability of mean flow velocity at the spark is important, with a factor of 2 between the maximum and minimum level. The cycle exhibiting the smallest mean velocity is cycle 15, which is the slowest combustion cycle. Cycles 2 and 10 exhibit very similar levels, but lowers than the one predicted for cycle 11, which is one of the fastest cycles. Fig. 15 compares isosurfaces of premixed flame progress variable colored by temperature for cycles 11 and 15, at 16 CAD after spark ignition. A vortex pushes the flame kernel of cycle 15 down towards the piston. As a result, the ensuing propagation appears to be slowed down as compared to cycle 11. In the latter, a high horizontal flow velocity favors the horizontal propagation of the flame, which interacts much later with the piston. All these observations points out that ignition and flame propagation are more influenced by the velocity magnitude at the spark plug and the direction of the flow in the combustion chamber than by cyclic variability of equivalence ratio.

Methodology for simulating the spark timing sweep

A spark timing sweep covering eight ignition times is available in the experimental database. Six of them are simulated in LES, respectively -7.51 CAD, -6.76 CAD, -5.26 CAD, -3.76 CAD, -2.25 CAD before the reference ST and the reference one. The strategy followed to perform the

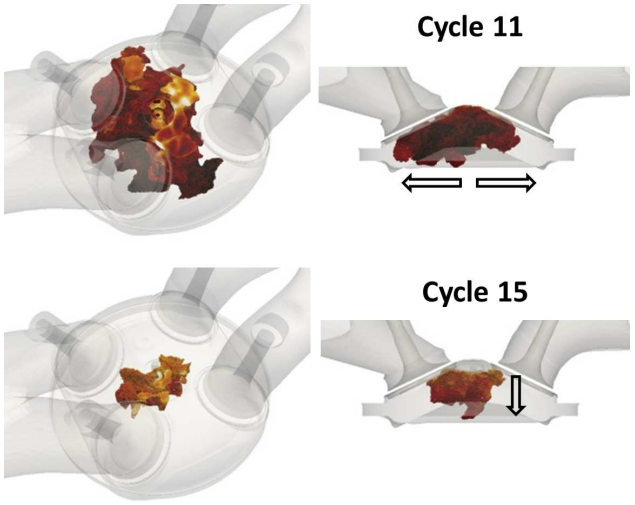

Figure 15. Evolution of the flame kernel at 16 CAD after spark ignition for the slowest (cycle 15) and the fast (cycle 11). Arrows indicates the main direction of flame propagation.

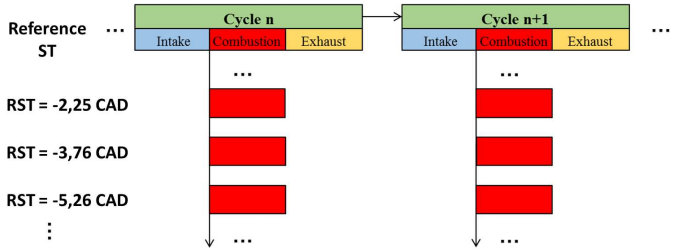

Figure 16. Illustration of the methodology used to simulate the spark timing sweep. Only combustion phases are simulated for the different spark timings, starting from the aerodynamic fields obtained from the reference case.

LES study of the ST sweep is illustrated in Fig. 16. In an approach already proven accurate in the past [6], the fifteen full consecutive LES cycles at the reference ST are used to yield initial conditions just before ignition for the studied ST. As a result only the combustion phases need to be computed. Several cycles can thus be simulated in parallel allowing reducing return times.

This approach is justified in the absence of dependency between consecutive cycles, which was verified for the reference spark timing of the studied engine and supposed to be valid also for all studied ST. This assumption may not be valid in the general case.

Analysis of the spark timing sweep

Fig. 17 to Fig. 19 compare the in-cylinder pressure predicted by the 15 LES cycles (black lines) with the 500 experimental cycles (brown lines) for three of the simulated ST. The LES cycles are able to reproduce the experimental pressure envelope recorded at the cylinder head whatever the spark timing (results for the ST not presented here have the same good agreement).

To go further on the analysis of in-cylinder pressure, the evolution of the coefficient of variation (COV) of the maximum pressure is presented on Fig. 20 for the whole spark timing sweep. The COV is defined as the ratio of the standard deviation to the mean of the maximal in-cylinder

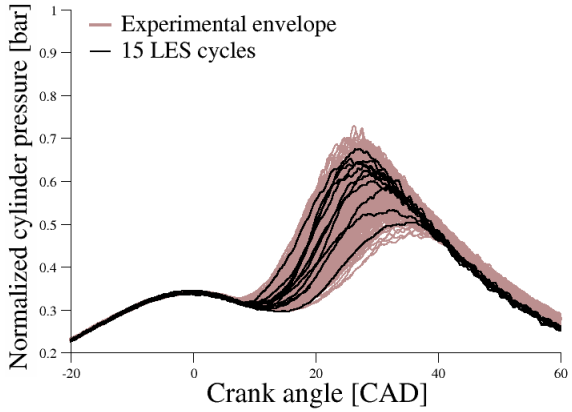

Figure 17. Temporal evolution of normalized in-cylinder pressure at a relative spark timing (RST) of -2.25 CAD.

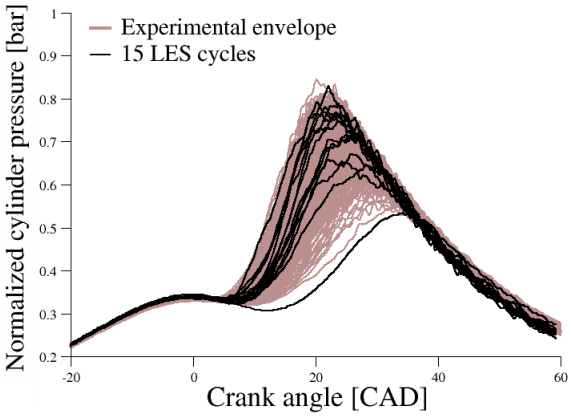

Figure 18. Temporal evolution of normalized in-cylinder pressure at a RST of -5.26 CAD.

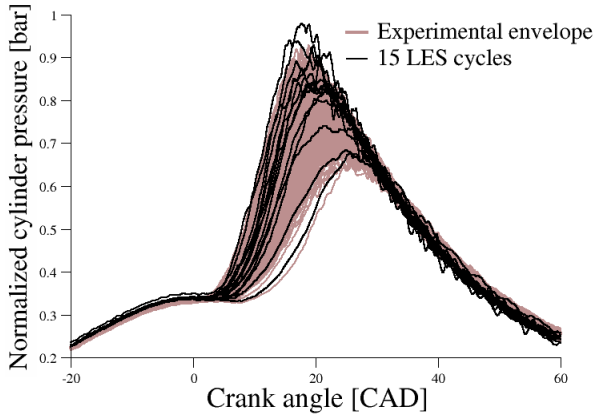

Figure 19. Temporal evolution of normalized in-cylinder pressure at a RST of -7.51 CAD.

pressure. The slight increase of the COV percentage for the

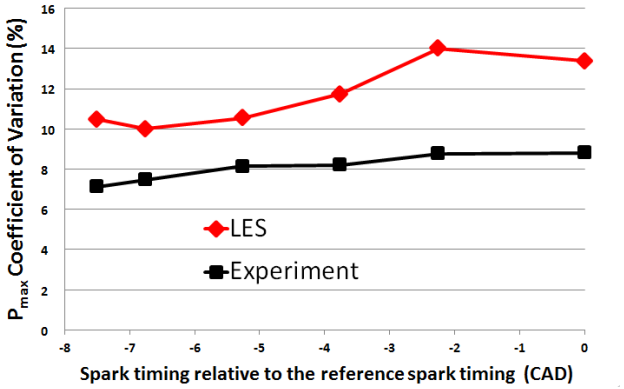

Figure 20. Evolution of the coefficient of variation (COV) of the maximum pressure on the whole spark timing sweep.

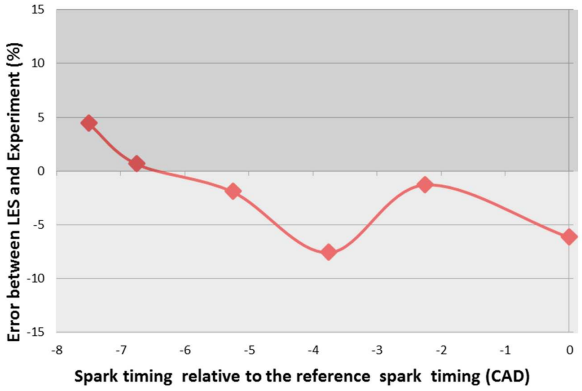

Figure 21. Combustion duration error over the relative spark timings.

latest spark timing is well reproduced by the LES, even if the numerical results overestimate a bit experimental ones, mainly due to the limited sample of LES cycles.

To compare combustion velocities between LES and experiment, the time Δt to go from 10% (CA_{10}) to 90% of burned mass in the combustion chamber (CA_{90}) is computed:

$$\Delta t = CA_{90} - CA_{10} \tag{11}$$

Fig. 21 shows the resulting mean error ϵ between LES results and experimental findings for the simulated ST, computed as:

$$\epsilon = \frac{\Delta t_{Exp.mean} - \Delta t_{LESmean}}{\Delta t_{Exp.mean}} \tag{12}$$

where the respective mean values are computed as an ensemble average of the available cycles (15 in LES, 500 in experiments). The maximum error is around 8%, confirming a good reproduction by LES of the experimentally observed combustion speeds. LES is found to underestimate it for the early ST, and to overestimate it for the latest spark timing. The reasons for this have not yet been further investigated.

Focusing on knock, the use of models ECFM-LES and TKI-LES allows to follow distinctly the propagation of the premixed flame initiated at the spark plug and the autoignition spots. Fig. 22 illustrates the knock occurrence

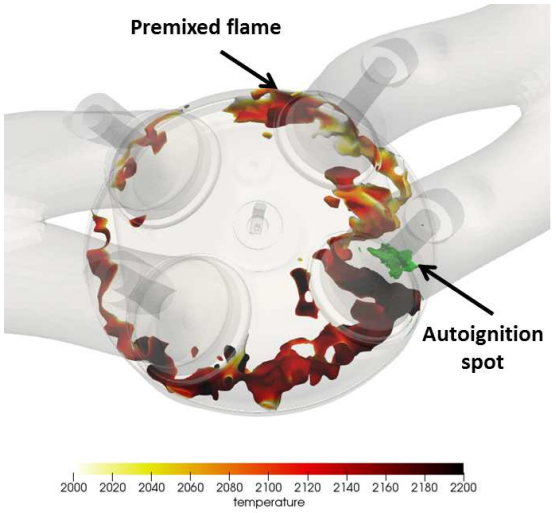

Figure 22. Autoignition spot (green) for LES cycle n°12 at +18 CAD after TDC. Premixed flame position is computed using a contour of ECFM progress variable colored by temperature.

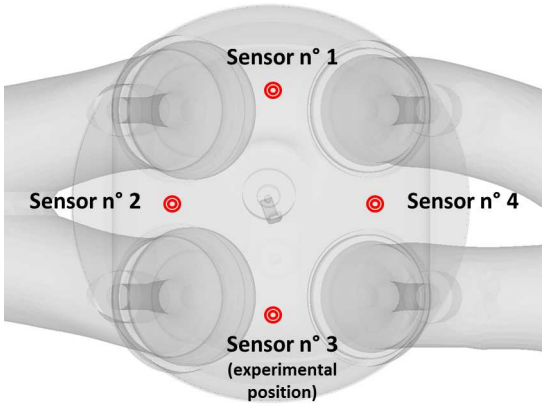

Figure 23. Localization of the four numerical sensors on the cylinder head.

for the LES cycle n°12 at a RST of -7.51 CAD. Premixed flame position is computed using a contour of ECFM progress variable colored by temperature, whereas autoignition spot is represented by a green contour of TKI progress variable. For this cycle, the premixed flame propagation is slow down in a rich region (equivalence ratio field not shown here) under exhaust valves giving much more time to fresh gases to autoignite. Such analysis allows to validate the occurrence of autoignition in the engine but can only be done for numerical results. As the aim here is to compared LES knock results to experimental ones, and because knock is characterized by pressure oscillations, fluctuation of pressure traces available both for LES and experiment are now analyzed.

From Fig. 12 and Fig. 17 to Fig. 21, the pressure fluctuation amplitudes increase when spark timing occurs more and more early during the cycle. To quantify this qualitatively accurate tendency predicted by LES, a Maximum Amplitude of Pressure Oscillations analysis currently (MAPO) (24) is conducted. This analysis is based on the pressure signal, the same numerical treatment being applied to LES and experimental signals.

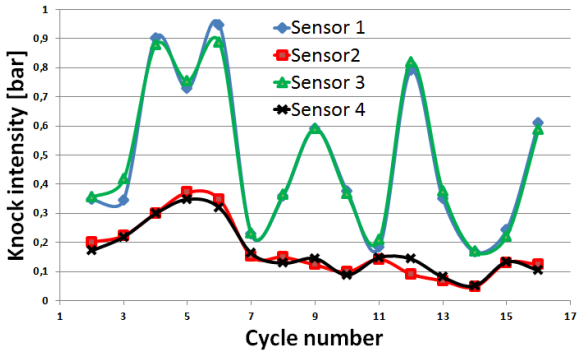

Figure 24. MAPO analysis of the pressure signal recorded at different sensor locations.

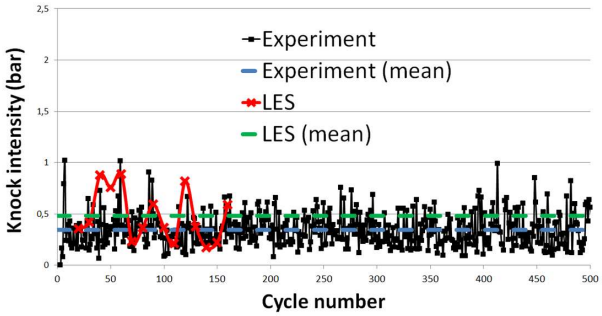

Figure 25. Knock intensity comparisons between LES and experiment at the reference ST. Mean knock intensity level is 0.34 bar for experiment and 0.37 bar for LES.

First, a sensitivity study of the MAPO results on the location of the pressure sensor is conducted using LES signals. To this purpose, three other numerical sensors are located between the valves as presented in Fig. 23.The MAPO analysis is conducted on these four probes for the fifteen LES cycles at the reference spark timing. Fig. 24 shows the resulting dependency of the knock intensity on the 15 cycles as a function of the position pressure recording. It reveals the existence of two groups with different values of knock intensity. Sensors n°1 and n°3 show equivalent knock intensity, much higher than knock intensity level predicted with sensors n°2 and n°4. This observation underlines the important sensitivity of pressure sensor location on the cylinder head.

In what follows, the MAPO analysis concerns the signals recorded at sensor n°3, corresponding to the experimental location. In Fig. 25 to Fig. 27, the knock intensity is plotted over the cycle identification number. To make these plots more readable, and as the LES sample is much smaller than for experiments, the identification number for LES cycles is multiplied by 10 in these figures: so LES cycle 2 becomes cycle 20, LES cycle 3 become cycle 30 ... etc. Mean values are also plotted both for LES and experiment. For all spark timings, the knock intensity predicted by LES is in good agreement with the experimentally observed levels. Based on the mean knock level evolution, the earlier spark ignition occurs in the cycle, the higher the knock intensity is, both in the experiments and in the LES. Results are also consistent for the three other spark timings simulated in LES, but not presented in this paper.

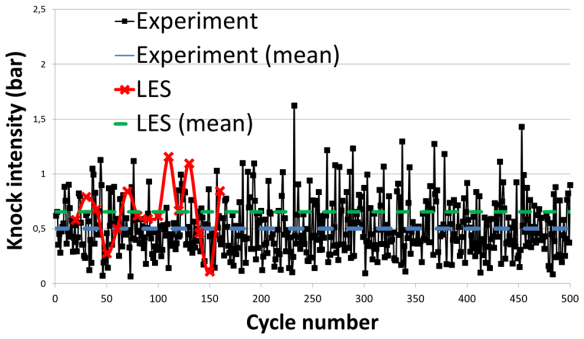

Figure 26. Knock intensity comparisons, ST is set to the reference minus 3.76 CAD. Mean knock intensity level is 0.5 bar for experiment and 0.59 bar for LES.

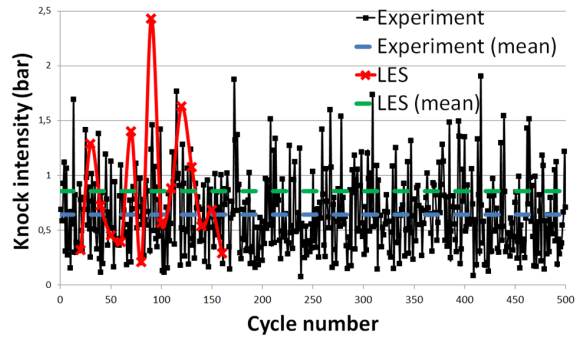

Figure 27. Knock intensity comparisons, ST is set to the reference minus 7.51 CAD. Mean knock intensity level is 0.64 bar for experiment and 0.85 bar for LES.

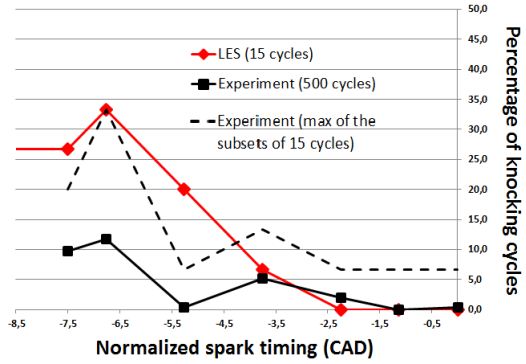

Figure 28. Percentage of knocking cycles over the relative spark timings for the common ST between experiment and LES.

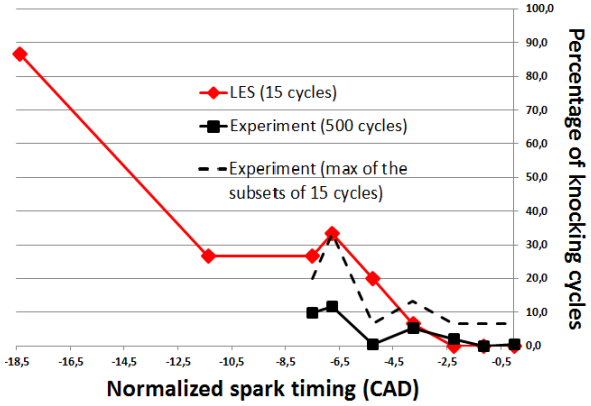

Figure 29. Percentage of knocking cycles over the relative spark timings for all the ST simulated in LES.

Another way to quantify the knock tendencies is to look at the percentage of knocking cycles. A cycle is considered as knocking when its knock intensity is superior to a threshold value defined on the real engine test bench. For the operating conditions of this study, the value of 1.1 bar is used both for LES and experiment. Fig. 28 shows the evolution of the percentage of knocking cycles over the relative spark timing (RST). As the sample of LES cycles is reduced, the experimental sample is divided randomly into subsets of 15 cycles for which the analysis is repeated, in addition to the full 500 cycles sample. The subset yielding the highest percentage is also plotted. At the reference ST (RST equal to zero), non knocking cycles are observed both for LES and experimental results. First knocking cycles are detected at -2.25 CAD before the RST in the experiment and at -3.76 CAD in the LES, with very comparable intensity level (around 5%). The main difference occurs at a RST of -5.26 CAD where the experimental level falls down close to zero, whereas LES predicts a continuous increase of the percentage of knocking cycles. The experimental behavior is quite puzzling and difficult to explain, but was not further explored here.

Two additional earlier ST have been simulated in LES, but weren't studied experimentally to avoid damages. The evolution of the percentage of knocking cycles is presented in Fig. 29. After a constant level until a RST of -11.3 CAD, LES predicts a sharp increase of the number of knocking cycles to reach a value close to 90%. This observation justifies the fact the real engine should not run with such early ST, for which the knock intensity (not shown here) increases sharply.

CONCLUSIONS

This paper presents for the first time a quantitative LES study of cyclic variability and knock taking into account direct fuel injection in a production four-valve spark ignition engine fueled with a typical European gasoline, and running at high load and speed. Particular attention has been paid to an accurate estimation of wall temperatures using a CHT study based on RANS calculations. Results of this CHT study were imposed as boundary conditions in LES. First, an analysis of the in-cylinder mixture preparation as a result of fuel injection and intake flow revealed that despite an early injection timing, the tumble motion is not able to mix air and fuel sufficiently fast to obtain a perfectly premixed mixture at spark timing. LES was shown to be able to reproduce the experimental cylinder pressure variation envelope using a limited sample of 15 simulated cycles, and this for all studied spark timings. Even if cycle-to-cycle variability is well predicted by LES, one LES cycle was found to lie below the experimentally reported envelope. A detailed analysis of the mean flow around the spark plug pointed out that cyclic equivalence ratio variability is limited and was probably not the main reason for cycle-to-cycle combustion variability. It was shown that ignition and flame propagation were more influenced by the velocity magnitude at the

spark plug, and by the cyclic variability of the flow during early flame propagation. To quantify knock intensity, the same MAPO analysis was applied to LES and experimental results. A sensitivity to the pressure sensor location on the cylinder head was conducted and showed that it strongly influenced the resulting knock intensity. This confirms that this location should be chosen with care for an on-board knock detection. The dependency of knock on spark timing was then analyzed. LES was shown to reproduce quite accurately the experimental findings in terms of intensity and percentage of knocking cycle's variation with spark timing. Future work concerns the exploration of the causes of cyclic variability and knock, in an attempt to identify control parameters allowing to reduce them in early design phases.

Acknowledgements

This work was funded by the GSM (Groupement Scientifique Moteur: groupe PSA, Renault SAS and IFP Energies nouvelles) and by ADEME (French Agency for Environment and Energy Control). The authors want to acknowledge Benoit ENAUX from groupe PSA for providing engine database and CHT calculation.

NOMENCLATURE

AI : auto-ignition
TDC: Top Dead Center
ST : Spark timing
RST : Relative Spark Timing
CHT : Conjugated Heat Transfer
MAPO : Maximum Amplitude of Pressure Oscillations

References

[1] Lafossas FA, Castagne M, Dumas JP et al. Development and validation of a knock model in spark ignition engines using a CFD code. *SAE Paper 2002-01-2701*, 2002; .

[2] Corti E and Forte C. Combination of in-cylinder pressure signal analysis and CFD simulation for knock detection purposes. *SAE Paper 2009-24-0019*, 2009; : 368–380.

[3] Lecocq G, Richard S, Michel JB et al. A new LES model coupling flame surface density and tabulated kinetics approaches to investigate knock and pre-ignition in piston engines. *Proc Combust Inst* 2011; 33(2): 3105 – 3114.

[4] Fontanesi S, Paltrinieri S, D'Adamo A et al. Knock tendency prediction in a high performance engine using LES and tabulated chemistry. *SAE Paper 2013-01-1082* 2013; 6: 98–118.

[5] Misdariis A, Vermorel O and Poinsot T. LES of knocking in engines using dual heat transfer and two-step reduced schemes. *Combustion and Flame* 2015; 162(11): 4304 – 4312.

[6] Robert A, Richard S, Colin O et al. LES prediction and analysis of knocking combustion in a spark ignition engine. *Proc Combust Inst* 2014; 35(3): 2941–2948.

[7] Robert A, Richard S, Colin O et al. LES study of deflagration to detonation mechanisms in a downsized spark ignition engine. *Combustion and Flame* 2015; 162(7): 2788 – 2807.

[8] Truffin K, Angelberger C, Richard S et al. Using large-eddy simulation and multivariate analysis to understand the sources of combustion cyclic variability in a spark-ignition engine. *Combustion and Flame* 2015; 162(12): 4371 – 4390.

[9] Poinsot T and Lele SK. Boundary conditions for direct simulations of compressible viscous flows. *Journal of Computational Physics* 1992; 101(1): 104 – 129.

[10] Moureau V, Lartigue G, Sommerer Y et al. Numerical methods for unsteady compressible multi-component reacting flows on fixed and moving grids. *Journal of Computational Physics* 2005; 202(2): 710 – 736.

[11] Gourdain N, Gicquel L, Montagnac M et al. High performance parallel computing of flows in complex geometries - Part 1: Methods. *Computational Science & Discovery* 2009; 2.

[12] Lax PD and Wendroff B. Systems of Conservation Laws. *Communications on Pure and Applied Mathematics* 1960; 13: 217–237.

[13] Smagorinsky J. General circulation experiments with the primitive equations. I: The basic experiment. *Mon Weather Rev* 1963; 91(3): 99–164.

[14] Schmitt P, Poinsot T, Schuermans B et al. Large-eddy simulation and experimental study of heat transfer, nitric oxide emissions and combustion instability in a swirled turbulent high-pressure burner. *Journal of Fluid Mechanics* 2007; 570: 17–46.

[15] Garcia M, Riber E, Simonin O et al. Comparison between Euler/Euler and Euler/Lagrange LES approaches for confined bluff-body gas-solid flow prediction. In *International Conference on Multiphase Flow 2007*.

[16] Iafrate N, Michel JB and Cuenot B. A study of gasoline multi-hole injector spray dynamics using LES. In *ILASS conference 2014*.

[17] Richard S, Colin O, Vermorel O et al. Towards Large Eddy Simulation of combustion in spark ignition engines. *Proc Combust Inst* 2007; 31: 3059 – 3066.

[18] Vermorel O, Richard S, Colin O et al. Towards the understanding of cyclic variability in a spark ignited engine using multi-cycle LES. *Combustion and Flame* 2009; 156(8): 1525 – 1541.

[19] Yahyaoui M, Truffin K and Pires Da Cruz A. *IDETHANOL project : corrélation des vitesses de flamme laminaires des mélanges essence/éthanol* . Technical report, 61272, IFP Energies nouvelles, 2009.

[20] Colin O and Truffin K. A spark ignition model for large eddy simulation based on an FSD transport equation (ISSIM-LES). *Proc Combust Inst* 2011; 33(2): 3097 – 3104.

[21] Colin O, Pires Da Cruz A and Jay S. Detailed chemistry-based auto-ignition model including low temperature phenomena applied to 3-D engine calculations. *Proc Combust Inst* 2005; 30: 2649–2656.

[22] Mehl M, Pitz W, Westbrook C et al. Kinetic modeling of gasoline surrogate components and mixtures under engine conditions. *Proc Combust Inst* 2011; 33(1): 193 – 200.

[23] Kuo K. *Principles of combustion (2nd ed.)*. John Wiley, New York, 1986.
[24] Zhen X, Wang Y, Xu S et al. The engine knock analysis - An overview. *Applied Energy* 2012; 92(Supplement C): 628 – 636.

Copyright